www.elsevier.com/locate/dsr2

The distribution of pelagic sound scattering layers across the southwest Indian Ocean

Philipp H. Boersch-Supan, Alex D. Rogers, Andrew S. Brierley

PII: S0967-0645(15)00225-8
DOI: http://dx.doi.org/10.1016/j.dsr2.2015.06.023
Reference: DSRII3919

To appear in: *Deep-Sea Research II*

Received date: 28 October 2014
Revised date: 13 May 2015
Accepted date: 23 June 2015

Cite this article as: Philipp H. Boersch-Supan, Alex D. Rogers, Andrew S. Brierley, The distribution of pelagic sound scattering layers across the southwest Indian Ocean, *Deep-Sea Research II,* http://dx.doi.org/10.1016/j.dsr2.2015.06.023

The distribution of pelagic sound scattering layers across the southwest Indian Ocean

Philipp H. Boersch-Supan[1,2,3,*], Alex D. Rogers[2], Andrew S. Brierley[1]

1. Pelagic Ecology Research Group, Scottish Ocean Institute, University of St Andrews, Fife KY16 8LB, UK

2. Department of Zoology, University of Oxford, Oxford OX1 3PS, UK

3. Present address: Department of Integrative Biology, University of South Florida, Tampa, Florida 33620, USA

* philipp@boersch-supan.de

Abstract

Shallow and deep scattering layers (SLs) were surveyed with split-beam echosounders across the southwest Indian Ocean (SWIO) to investigate their vertical and geographical distribution. Cluster analysis was employed to objectively classify vertical backscatter profiles. Correlations between backscatter and environmental covariates were modelled using generalized additive mixed models (GAMMs) with spatial error structures. Structurally distinct SL regimes were found across the Subantarctic Front. GAMMs indicated a close relationship between sea surface temperature and mean volume backscatter, with significantly elevated backscatter in the subtropical convergence zone. The heterogeneous distribution of scattering layer biota reflects the biogeographic zonation of the survey area and is likely to have implications for predator foraging and carbon cycling in the Indian Ocean.

1 Introduction

Pelagic biota in the open ocean are structured at a broad range of spatial and temporal scales (Haury et al., 1978; Steele, 1978). Abundance and assemblage composition vary on scales from millimetres, to miles, to entire ocean basins. Temporal variation encompasses minutes to decades, incorporating daily patterns such as diel vertical migration (Angel, 1985), seasonal cycles (Urmy et al., 2012; Cisewski et al., 2010) and inter-annual trends (O'Driscoll et al., 2009). There are numerous physical and biological drivers of this heterogeneity including temperature, mixing, current patterns, predator density and food availability.

A substantial proportion of biomass below the photic zone is concentrated in so-called sound scattering layers (SLs) which have been observed since the invention of echosounders in the mid 20th century (Christensen et al., 1946; Lyman, 1947). Scattering layer assemblages encompass species from diverse taxa such as myctophid and stomiiform fish, squid, decapod shrimps and various groups of gelatinous zooplankton (Farquhar, 1977; Bradbury et al., 1970; Pakhomov and Froneman, 2000). SLs often contain high species diversity (e.g. Kemp et al., 2014; Letessier et al., 2014, this issue) and, as a result, species discrimination and consequently direct biomass estimation are usually not possible from acoustic data alone. Nonetheless backscatter data, particularly when available at multiple acoustic frequencies, can provide rich ecological information. From the very early decades of scattering layer research, attempts were made to link acoustic information with species-abundance and diversity data. For example, investigations were undertaken to determine whether pelagic biogeographical provinces were reflected in acoustic backscatter signatures (Backus and Craddock, 1977; Tont, 1976) and to examine possible effects of hydrographic features such as fronts and eddies on scattering layer structure and composition (Cole et al., 1970; Conte et al., 1986). More recently, distinct differences in the vertical structure and/or migration dynamics of pelagic SLs combined with faunal turnover have been observed

across mesoscale oceanographic fronts (Lara-Lopez et al., 2012; Ohman et al., 2013; Cox et al., 2013) and eddies (Godø et al., 2012), confirming that biogeographic patterns are not only reflected in backscatter spectra but also the vertical organisation of scattering layers.

A large proportion of scattering layer biomass undertakes diel vertical migrations (DVM), generally moving from the mesopelagic zone (200-1000 m) into more productive near-surface waters at night, and returning to depth at dawn. This behaviour is thought to arise as a means for individuals to avoid visual predators near the illuminated surface in daylight and forage near the surface at night (Pearre, 2003). Vertical migrators play an important role in marine food-webs because they link surface primary production to higher trophic levels, but also in marine biogeochemical cycles because they actively contribute to the downward flux of nutrients and particulate organic matter (Hidaka et al., 2001; Al-Mutairi and Landry, 2001; Steinberg et al., 2008). Both aspects have only recently been incorporated into global models of the Earth system (Lehodey et al., 2010; Bianchi et al., 2013) and there is a need for a better understanding of biomass distributions and migration dynamics as inputs into these ecosystem models. At the most basic level there is a requirement for better data on the global standing stock of scattering layer biota: recent acoustic and modelling studies suggest that the global biomass of mesopelagic fish may have been underestimated by an order of magnitude or more (Kloser et al., 2009; Kaartvedt et al., 2012; Irigoien et al., 2014).

SL organisms are predated upon by a diverse set of oceanic nekton, including species of commercial interest such as tuna and billfish (Potier et al., 2007, 2005), marine mammals (Naito et al., 2013; Arranz et al., 2011, Boersch-Supan et al. 2012) and species of conservation concern such as oceanic sharks (Howey-Jordan et al., 2013). Trophic interactions between scatterers and their predators are constrained in space and time by the vertical SL structure and SL migration dynamics on one hand, and the diving capabilities of the predators on the other. Along the continental slope and near oceanic

islands and seamounts abrupt topography can mediate predator-prey relationships, as SL organisms can become trapped on these physical features by being blocked on their vertical descent (Isaacs and Schwartzlose, 1965) and/or as a result of diverse flow-topography interactions (Genin, 2004). Migration by SL species may import water-column biomass to the sea bed, facilitating rich benthic communities (Genin et al., 1986; Rowden et al., 2010) as well as substantial aggregations of high trophic level biota around seamounts (Tseytlin, 1985; Koslow, 1997; Morato et al., 2008, 2009), of which the latter are targeted globally by commercial fisheries (Pitcher et al., 2010).

Despite the vast expanse of mid-ocean ridge systems, and the ubiquity of seamounts in the global ocean (Yesson et al., 2011; Kim and Wessel, 2011), little is known about the influence of these topographic features on pelagic scattering layers and, ultimately, oceanic food-webs and biogeochemical cycles at a global scale. While locally enriched biomass has been observed, Priede et al. (2013) suggested that, on a basin scale, ridges have a neutral effect on biomass per unit area, as the increased benthic biomass on topographic features is balanced by the displacement of pelagic biomass by the topography itself (the presence of the ridge prevents the presence of water volume). Opdal et al. (2008) describe scattering layers along the northern Mid-Atlantic Ridge and possible topographical, hydrographical and biological processes shaping them. They report increased pelagic backscatter above a fracture zone that coincides with the northern Sub-polar Front. Cox et al. (2013) used multi-frequency acoustic data to estimate epipelagic (<200 m) zooplankton biovolumes and scattering classes across the same front. Their acoustic observations suggest a change in the species composition of the pelagic community across the Sub-polar Front, but do not detect an across-ridge difference in biovolumes.

Apart from a largely descriptive study of the influence of scattering layer structure on elephant seal foraging (Boersch-Supan et al., 2012), little research has been conducted on the large scale distribution of scattering layers in the Southern Indian Ocean or along the Southwest Indian Ridge (SWIR). The study

presented here intends to fill that gap, by describing the distribution of pelagic SLs and their vertical structure across the SWIO and by exploring their variability with respect to latitudinal environmental gradients. An understanding of the influence on scattering layers of the regional oceanography and the ridge as a whole is not just important for understanding ecological and biogeochemical processes in the SWIO at the basin scale, but also as a background to understanding local-scale interactions (c. 10 km) between pelagic biota and individual seamounts.

Fisheries acoustic data possess a number of properties which make their statistical analysis challenging. These include patchiness, scale dependency and spatio-temporal correlation. Modelling acoustic data in a statistically appropriate matter is therefore not trivial, and there remains a lack of appropriate analytical tools (Ciannelli et al., 2008). Spatio-temporal correlation is particularly pertinent for observations of oceanic SLs, with their continuous extent over large geographic distances, and their often complex vertical migration cycles. Acoustic data are usually collected at high sampling rates (0.1-10 Hz) and commonly binned into sampling units with a horizontal scale of c. 1 km. Individual sampling units along a vessel's trajectory are therefore highly correlated in space and time. Furthermore space and time are usually confounded in collected data opportunistically, where the movement of the vessel is largely determined by other objectives such as fishing or other surveying tasks and replicates are seldom collected at any one location. Spatial auto-correlation violates the usual assumption of independence between data points and if not accounted for leads to the underestimation of standard errors, and elevated type I errors (Legendre, 1993).

Acoustic survey data are widely employed in routine stock assessments (Fernandes et al., 2002) and a variety of statistical approaches are employed both in survey planning and data analysis to estimate and minimize the effects of non-random sampling in space (e.g. Rivoirard et al., 2000; Petitgas, 2001). Most scattering layer studies, however, have not addressed the issue of spatio-temporal correlation in a

systematic fashion. A substantial proportion of the literature is largely descriptive (e.g. Opdal et al., 2008; Klevjer et al., 2012), while the more quantitative studies tend to address autocorrelation by averaging over space and/or time (e.g. Godø et al., 2012) or reducing spatially explicit observations to derived indices (e.g. Burgos and Horne, 2008; Urmy et al., 2012), resulting in the loss of information, and complicating the transfer of results into the parameterisation of spatio-temporally explicit ecosystems models. Some studies do not address the issue of spatial autocorrelation at all (e.g. Hazen and Johnston, 2010).

Over the past decade generalized additive models (GAMs; Wood 2006) have gained popularity for modelling non-linear relationships between acoustic backscatter and environmental variables (e.g. Zwolinski et al., 2009; Hazen and Johnston, 2010; Murase et al., 2013). GAMs are non-parametric extensions of generalized linear models, with a linear predictor involving a sum of smooth functions of covariates. The advantage of a GAM over the explicit specification of non-linearities e.g. in a non-linear least squares framework, is that no *a priori* functional relationship between response and dependent variable has to be assumed. GAMs are data-driven and the data determine the nature and smoothness of the relationship between response and predictors. Cross-validation or likelihood-based methods are employed to prevent over-fitting (Wood, 2006). These methods, however, rely on independent observations, and will not perform adequately when confronted with non-independent observations. In such cases there is a risk that an overly-complex smooth term is fitted, leading to false estimates of the functional relationship between a predictor and the dependent variable, as well as the associated confidence intervals (Ciannelli et al., 2008).

In this study correlations between environmental variables and backscattering strength are explored using a modelling framework based on linear mixed models (Pinheiro and Bates, 2000) that incorporates

spatial correlation structures, while retaining the flexibilities of GAMs. As such, it provide a step forward in use of fishery acoustic data for ecosystem modelling.

2 Materials and Methods

2.1 Data collection

Basin-scale observations of acoustic backscatter were made from two research vessels (*RV Dr. Fridtjof Nansen*, DFN; *RSS James Cook*, JCO) and three fishing vessels in the period between November 2009 and April 2012. Data from the research vessels were collected for the purpose of this study, while the data from fishing vessels were collected as part of the Australian Integrated Marine Observing System's Bio-Acoustic Ship Of Opportunity Programme (IMOS; Ryan, 2011). IMOS data were obtained through the IMOS Ocean Portal (`http://imos.aodn.org.au/imos/`) as mean echointegrated volume backscattering coefficient (s_v (m^{-1}); MacLennan et al., 2002) for cells of 1000 m distance and 10 m depth to a max depth of 1000 m.

Data from fishing vessels were collected using Simrad ES60 echosounders (Kongsberg Maritime AS, Horten, Norway) operating at 38 kHz, while the research vessels employed Simrad EK60 echosounders operating at 38 kHz and 18 kHz. All echosounders were calibrated following the recommendations of Foote et al. (1987), and accounting for the systematic triangle wave error that is embedded in ES60 data (Ryan and Kloser, 2004). Calibration parameters for DFN and JCO are given in Table S1. All acoustic sampling was conducted while the vessels were in transit between sampling stations or fishing locations, usually at speeds around 5 ms^{-1}. Survey tracks are shown in Figure 1.

2.2 Acoustic data processing

Echoview software (Version 4.90, Myriax Pty Ltd, Hobart, Tasmania, Australia) was used to visualise acoustic data in the form of calibrated echograms. Transducer parameters were adjusted with reference to calibration data, and environmental parameters (sound speed and frequency-specific attenuation) were calculated from CTD data using algorithms of Fofonoff and Millard (1983). CTD data were averaged over c. 350 km long segments of the cruise track to account for geographic variation of environmental parameters across the study area. To ensure the comparability of the DFN and JCO data with the integrated backscatter data provided by IMOS, the acoustic post-processing followed the IMOS processing framework (Ryan, 2011), which involved filtering to remove intermittent noise spikes (Anderson et al., 2005), attenuated pings, persistent intermittent noise and finally background noise (De Robertis and Higginbottom, 2007).

Integrated mean volume backscatter (MVBS, S_v (dB re m^2); MacLennan et al., 2002) was exported as georeferenced cells of 1000 m distance and 10 m depth, to a maximum depth of 1000 m. IMOS MVBS data were converted into the log-domain using the relationship

$$S_v = 10\log_{10}(s_v). \quad (1)$$

Apparent solar time for every cell was calculated from midpoint longitude lo_i and UTC timestamp $t_{UTC,i}$ as

$$t_{local,i} = t_{UTC,i} + (lo_i/15)\times 3600 + EoT(t_{UTC,i}) \quad (2)$$

where *EoT* is the equation of time (Meeus, 1998) as implemented in the insol package for R (Corripio, 2013). Sunrise and sunset times were calculated using routines provided by the Maptools package (Lewin-Koh and Bivand, 2010). Cells were classified as day, night or twilight, where twilight was

defined as 1.5 hours before and after sunset and sunrise (Kloser et al., 2009), and into Austral Summer (October to March) or Austral Winter (April to September).

2.3 Environmental covariates

Concurrent measurements of acoustic backscatter and environmental parameters such as sea surface temperature and chlorophyll a fluorescence were available for the two research vessel cruises, but not for the IMOS data. To avoid a bias between the datasets in subsequent analyses all environmental parameters were sampled for each acoustic sampling unit from gridded data products based on remote-sensing observations of the sea surface. These predictors can only serve as habitat-proxies for SL organisms in deep water, as the environment at the sea surface is not experienced directly by the vast majority of SL organisms.

Sea surface temperature (SST) was sampled from the Operational Sea Surface Temperature and Sea Ice Analysis (OSTIA; Donlon et al., 2012) at a spatial resolution of 1/20°. Surface chlorophyll concentrations were sampled from GlobColour grids at a spatial resolution of 1/24° (Anon., 2010) using monthly model-averaged observations for case 1 water (CHL_1 parameter of GlobColour). Water depth was sampled from the GEBCO bathymetric grid at a resolution of 30 arc seconds (GEBCO, 2010). Sampling from gridded datasets was achieved using a combination of the netCDF operators (NCO Version 4.3.0; Zender, 2008) and the raster package for R (Hijmans and van Etten, 2012).

Distance to the ridge and distance to the nearest coastline were calculated using GRASS (Version 7.0.svn; Neteler et al., 2011) and the geosphere package for R (Hijmans et al., 2012). Spreading ridge axes were taken from Coffin et al. (1998). The axis of the Ninety East Ridge, as well as all shorelines were extracted from GEBCO bathymetry.

Remotely sensed SST and chlorophyll concentration were validated against *in situ* surface measurements of temperature and fluorescence made using an SBE 21 SeaCat thermosalinograph (Sea-Bird Electronics, Bellevue, WA, USA) during the two research vessel cruises. OSTIA SST showed a consistent positive offset of about 1°C across the measured SST range, but was otherwise in very close agreement (Pearson's r=0.994, Fig. S1A). GlobColour monthly averaged chlorophyll concentrations correlated reasonably well with *in situ* fluorescence measurements (Pearson's r=0.536, Fig. S1B). The weaker correlation between the two chlorophyll measures is likely the result of a strong diel fluctuation of the *in situ* fluorescence signal, which is an artefact of physiological and photochemical effects rather than an indication of biomass fluctuations (Falkowski and Kolber, 1995).

2.4 Statistical analyses

Analyses were performed using the R environment for statistical computing (Version 2.14; R Development Core Team, 2010).

2.4.1 Cluster analysis

Vertical S_v profiles were subjected to cluster analysis in an attempt to objectively classify scattering layer regimes with differing vertical structures. Unconstrained clustering was achieved using *k*-medoids clustering with the partitioning-around-medioids algorithm (PAM; Kaufman and Rousseeuw, 1990) as implemented in the cluster package for R (Maechler et al., 2012). PAM was run on dissimilarity matrices based on euclidean distances as well as the general dissimilarity coefficient of Gower (1971, see suppl. methods for details). Goodness of clustering for different prespecified numbers of clusters *k* was assessed using the overall average silhouette width $s(k)$ (Rousseeuw, 1987, see suppl. methods for details).

2.4.2 Statistical modelling

Generalised additive mixed models (GAMMs; Wood, 2006) were used to investigate possible relationships between environmental variables and backscattering strength at different frequencies in different depth strata . GAMMs enable the inclusion of correlation structures to model the inherent autocorrelation of acoustic survey data. Models were fit using different combinations of explanatory variables, and final models for each response were selected by Akaike's information criterion (AIC; Akaike, 1973). Where multiple models had similarly low AIC scores and did not show significant differences in a likelihood ratio test, the more parsimonious model was selected. Time of day was modelled using a cyclic regression spline. Autocorrelation of residuals was modelled using a first-order autoregressive error structure (AR(1); Pinheiro and Bates, 2000). The AR(1) model was nested within individual survey legs. Models were fit to integrated backscatter between the surface and 200 m (shallow scattering layer; SSL) and between 200 m and 1000 m (deep scattering layer; DSL) using an identity link function and Gaussian errors.

3 Results

A total of 33,406 km of survey track were analysed in this study, comprised predominantly of 38 kHz data. 6,295 km of survey track also included observations at 18 kHz. A detailed overview of the data sources and their distribution with respect to echosounder frequency, season and time of day is provided in Table 1. Representative echograms for the areas north and south of the Subantarctic Front and the corresponding vertical backscatter profiles are shown in Figure 2.

Survey coverage from JCO was sparse, as interference from geophysical and oceanographic echosounders, as well as bubble entrainment under the JCO's hull (Butler, 2009) severely degraded data quality. Both factors resulted in the rejection of over 80% of the collected pings during initial processing.

3.1 Vertical structure

Variations in the vertical backscatter structure were examined using cluster analysis. Average silhouette widths indicated weak structure ($s(k)$≈0.25; Nagpaul, 1999) and favoured a two cluster solution in all cases. Partitions based on Gower's similarity coefficient had consistently higher $s(k)$ values than those based on euclidean distances, indicating tighter clustering (Fig. S2).

3.1.1 38 kHz data

For the 38 kHz dataset the composition of the two-cluster partitions differed markedly between the two underlying dissimilarity metrics. The two clusters based on euclidean distances (E1, E2; Fig. 3A) cover the entire geographical range of the data, but their composition with respect to time-of-day is distinct. Cluster E1 contains mostly daytime samples and cluster E2 mostly nighttime samples (Fig. S3A). The vertical backscatter profiles differ the most in the top 400 m of the water column (Fig. 4A), with the night time cluster E2 exhibiting increased backscatter in this depth interval. The two 38 kHz clusters based on Gower's distances (G1, G2; Fig. S3B) are largely indistinguishable with respect to time-of-day, but are well separated in geographic space (Fig. 3B). Cluster G2 occupies the latitudinal centre of the survey area (32°S-42°S), while cluster G1 is geographically discontinuous and occupies the northern (<32°S) and southern (>42°S) edges of the survey area. The largest difference in the backscatter profiles is found between 200 m and 700 m depth (Fig. 4B), with mid-latitude cluster G2 exhibiting elevated backscatter in this depth interval, as well as a slight upward shift of the shallow S_v maximum in G2 to approx. 50 m. Based on the bimodal latitudinal distribution, G1 can be separated into two subclusters (G1a, G1b; Fig. 4C), both of which show less backscatter than the central cluster. The depth profile of the northern cluster G1a shows a distinct shallow and deep scattering layer, which is similar to the layer structure in G2, whereas the layer structure in the south (G1b) is quite distinct indicating several, less pronounced sub-layers.

3.1.2 18 kHz data

For the 18 kHz data the k=2 partitions for both dissimilarity measures resulted in a day-night split. In an attempt to extract a possible geographic structure the dataset was subdivided into daytime and nighttime S_v profiles and subjected to separate PAM analyses based on Gower dissimilarities (Fig. S2C), as clusters based on this distance measure had higher $\bar{s}(k)$ values compared to euclidean distances. Spatially separated clusters were obtained for both time periods, with a North-South divide near 35°S in both cases (Fig. 3C,D). Daytime S_v profiles differed between the two clusters in the depth of the subsurface S_v maximum (Fig. 4D). In the northern cluster D1 deep backscatter peaks around 400 m, whereas D2 exhibits a peak some 50 m shallower as well as elevated backscatter in the surface layer. Nighttime S_v profiles differed in backscattering strength below 100 m, with consistently lower levels in the Northern cluster N2. A short segment of a transect near 42°S 48°E was classified as belonging to the northern cluster N2 (Fig. 3D). S_v profiles in this segment differed from the remainder of cluster N2 by the presence of two deep S_v maxima near 100 m and 500 m depth, respectively (Fig. 4F).

3.2 Environmental drivers of backscattering strength

Temperature and time of day consistently emerged as important predictors in all models, while chlorophyll concentration was the only predictor that was not included in any of the final models. The correlation coefficient ϕ of the AR(1) error structure was close to 1 in all cases, indicating strong positive autocorrelation among the residuals. Empirical variograms showed increasing semivariance up to a range of approx. 100 km (Fig. S4).

3.2.1 38 kHz data

The final model for S_v:**DSL38**, the backscatter from the DSL at 38 kHz included smooths of SST (stratified by season), time of day and distance to the nearest shoreline (r^2_{adj}=0.35, AIC=38 418, ϕ=0.985; Table 2, Fig. 5). Model output showed that variations in SST across the survey area had the largest effect on S_v:**DSL38**. During Austral Summer the deep scattering layer exhibits a pronounced backscatter maximum at approximately 18°C and then drops off substantially towards colder temperatures (Fig. 5A). Model predictions for the Winter have much larger standard errors at the extremes of the sampled temperature range, but the model exhibits a local S_v:**DSL38** maximum at 14°C (Fig. 5B). Time of day shows a weaker effect on S_v:**DSL38**, with a minimum around 03:00 hrs local time and peaks during local daytime (Fig. 5C). Distance to shore proved to be a highly significant predictor during model selection and show moderate effect sizes and a complex relationship with S_v:**DSL38** (Fig. 5D).

The final model for backscatter from the SSL at 38 kHz (S_v:**SSL38**) included a linear depth term and smooths of SST (stratified by season), time of day, and distance to the nearest ridge (r^2_{adj}=0.66, AIC=100 150, ϕ=0.936; Table 2, Fig. 6). Again, SST showed the largest effect on backscatter, although for the SSL there is a general trend of decreasing S_v:**SSL38** with temperature (Fig. 6A-C). Two local maxima appear during summer near 17°C and 8°C, while during winter there is a pronounced local minimum at 13°C and a local maximum at 9°C. Time of day showed a pronounced effect with elevated backscatter at night time, peaking just before and just after midnight and a local maximum during noon (Fig. 6D). The influence of water depth was weak, with S_v:**SSL38** increasing linearly towards shallower depths (Fig. 6E), and the distance to ridge term showed fairly stable levels of backscatter within 500 km of a ridge followed by a slight decrease (Fig. 6F).

3.2.2 18 kHz data

The final model for S_v:**DSL18**, the backscatter from the DSL at 18 kHz, included smooths of SST, time of day (stratified by location on or off SWIR) and depth, and both distance measures (r^2_{adj}=0.73, AIC=15 380, ϕ=0.815; Table 2, Fig. 7). Model output showed that distance to the Ridge had the largest individual effect on S_v:**DSL38**, with a sharp increase at distances beyond 1200 km (Fig. 7E). Temperature also had a large effect with a local S_v:**DSL18** maximum at approximately 17°C followed by relatively high values towards colder temperatures and another rise in backscatter at temperatures below 10°C (Fig. 7A). Time of day showed a weaker effect on S_v:**DSL38**, that differed significantly at locations on the SWIR relative to elsewhere. In both cases, daytime backscatter was elevated relative to night time backscatter, with afternoon backscatter on the ridge being elevated relative to off the ridge (Fig. 7B,C). The influence of water depth is moderate at depths, with S_v:**SSL38** increasing linearly from 1500 m towards shallower depths (Fig. 7D). No depth effect was seen at depths beyond 1500 m. Distance to shore proved to be a highly significant predictor during model selection and show decreasing S_v:**DSL18** towards both extremes of the predictor range (Fig. 7F).

The final model for backscatter from the SSL at 18 kHz (S_v:**SSL18**) included smooths of SST, time of day (stratified by location on or off SWIR), and distance to the nearest ridge (r^2_{adj}=0.55, AIC=20 389, ϕ=0.943; Table 2, Fig. 8). Time of day showed the largest effect on backscatter. In both strata S_v:**SSL18** was elevated during the night, but while off the ridge backscatter remains low during the day (Fig. 8B), there is a secondary backscatter peak around noon on the ridge (Fig. 8C). There was a general trend of increasing S_v:**SSL18** with decreasing temperatures, with a local minimum at 20°C (Fig. 8A). The influence of water depth was comparably weak, with S_v:**SSL18** decreasing linearly from 3000 m towards deeper depths (Fig. 8D).

4 Discussion

4.1 Vertical structure

Clustering based on Gower's dissimilarities provided evidence of three structurally distinct scattering layer regimes for both frequencies. The approximate boundaries of these regions are along 32°S and 42°S, which roughly corresponds to the boundaries of the Subtropical convergence zone (SCZ). The northern and central regimes were structurally similar, both exhibiting a pronounced shallow and deep scattering layer, although the vertical positions of these layers are shifted upwards by 50–100 m in the SCZ. The scattering layer structure in the area south of 42°S was quite different, with backscatter being distributed more uniformly through the water column. These results confirm an earlier, descriptive analysis of scattering layer structure across the Subantarctic Front (Boersch-Supan et al., 2012), and are consistent with step changes in scattering layer structure observed across oceanographic fronts elsewhere (Cole et al., 1970; Lara-Lopez et al., 2012; Ohman et al., 2013). In particular, the shallowing of the daytime 18 kHz DSL south of the convergence is consistent with a faunal transition from species with larger swimbladders in the North to species with smaller swimmbladders in the South, which would shift the resonance depth upwards in the watercolumn. This matches observations from trawl samples, which feature the myctophid *Ceratoscopelus warmingii* and the hatchetfish *Argyropelecus aculeatus* as numerically dominant species in the North, whereas the smaller sternoptychid *Maurolicus muelleri* is dominant in the South (Kemp et al., 2014, this issue).

The Subtropical (STF) and Subantarctic Fronts (SAF) are thought to represent major biogeographic boundaries, dividing distinct faunal provinces in the southern Indian Ocean (Longhurst, 1998; Vierros et al., 2009). Previous research, as well as the biological sampling programme run concurrently to the acoustic surveys analysed in this study, exposes the role of the SAF as a faunal boundary across multiple

trophic levels from microbes and phytoplankton (Djurhuus et al., 2014; Bornman et al., 2014, both this issue) and macrozooplankton/micronekton (Pakhomov et al., 1994; Letessier et al., 2014, this issue) to cephalopods (Laptikovsky et al., 2014, this issue) and fish (Kemp et al., 2014, this issue). As both sound-scattering properties and vertical position in the water column can be taxon-specific properties, the drastic change in the vertical structure of the SLs is not surprising.

4.2 Backscatter and sea surface temperature

GAMM results indicated a strong effect of SST on the backscattering strength of both SSL and DSL. There was a pronounced local maximum in backscatter from the DSL at both observation frequencies in the surface temperature range indicative of the STF (14.5°-18.5°C and 11.5°-15.5°C in Austral Summer and Winter, respectively; Figs. 5A,B and 7A), and this S_v maximum appears to follow the seasonal shift of the STF axial temperature (Figs. 5A,B). Increased backscatter, as well as increased net-sampled macrozooplankton/micronekton biomass have also been observed in the SCZ south of Cape Agulhas (c. 20°E; Barange et al., 1998; Pakhomov et al., 1994), while no increase in acoustic backscatter was reported across the STF east of New Zealand, where the frontal temperature gradient is much shallower (McClatchie et al., 2004). Another local maximum in DSL backscatter appears in the axial temperature range of the SAF. This is more pronounced in the 18 kHz data (Fig. 7A) than in the 38 kHz data (Fig. 5B), and not evident for the Winter subset of the 38 kHz, where sparse observations lead to very large model uncertainty (Fig. 5B). Increased 18 kHz backscatter across a sub-polar front was also observed by Opdal et al. (2008) in the North Atlantic. The above results indicate that the effects on backscattering strength are not caused by temperature directly, but that SST is merely a proxy for frontal location, and the effects on backscattering strength is a result of multiple physical and biological processes at these fronts.

The pattern is not quite as clear for backscatter from the SSL. The 38 kHz backscatter generally decreases with temperature. The vertical S_v profiles for these data suggest that this might be an artefact caused by the shallowing of the SSL across the SCZ (Fig. 4B), resulting in the movement of scatterers into the so called surface dead zone, i.e. the part of the water column that is shallower than the downward-looking, hull-mounted echosounder transducer can sample (O'Driscoll et al., 2009). However, the S_v profile for 38 kHz backscatter south of the SAF (Cluster G1b, Fig. 4C) further suggests an actual decrease in surface backscatter in the southern part of the survey area. This might be reflected in the steeper decrease in S_v^{SSL38} south of the SAF (Fig. 6A), although it is difficult to estimate the relative contributions of both effects. 18 kHz backscatter from the SSL steadily increases across both frontal zones, which for the SAF matches the observations of Opdal et al. (2008) in the North Atlantic.

The southern hemisphere SCZ has been estimated to provide approximately 5% of the global net primary production in the oceans (Longhurst et al., 1995). If the results of Barange et al. (1998), Pakhomov et al. (1994) and this study are indeed indicative of elevated deep micronekton biomass across the SCZ in the southern Atlantic and Indian Ocean, a larger proportion of this production than previously considered may be actively exported to the deep ocean.

4.3 Ridge effect on backscattering strength

No compelling evidence could be found for an effect of the ridge on total backscatter intensity. An on ridge/off ridge factor variable was discarded during model selection, as it did not improve model fit, although stratifying the time-of-day smooth by this variable did improve both 18 kHz models. However, most 18 kHz samples within the SCZ were collected on the ridge, confounding potential effects of the frontal zone with those caused by the ridge. In fact, the cluster analysis does not provide evidence for distinct vertical structures between the ridge and elsewhere within the frontal zone (Figs. 3C,D). Depth and distance to the ridge were retained as a predictor in the 38 kHz SSL model (Fig. 6E). Distance to ridge

exhibited a negative effect at large distances from the ridge (>750 km), which applies to data sampled near the African continental shelf and in the wider vicinity of Kerguelen Plateau, suggesting no role of the ridges themselves in this result. Depth was the weakest predictor in this particular model and indicates slightly increased backscatter with decreasing depth. More convincing evidence for a ridge effect comes from the 18 kHz DSL model. Large effect sizes (>10 dB, equivalent to >10 fold on the linear scale) are predicted (Fig. 7E), although again, the biggest effect is predicted at ranges >1200 km from the ridge indicating effects of the African and/or Kerguelen shelf break, rather than from the SWIR. The model, does however predict a stepwise reduction of backscatter by approximately 3 dB, equivalent to a two-fold reduction on the linear scale, within 400 km of the ridge. Depth is also retained in the 18 kHz DSL model, with a strong positive effect (3 dB) at depths shallower than 1500 m. Generally, these results have to be treated with care, as both distance measures are rather crude metrics on a basin scale, potentially just capturing unexplained variation caused by unidentified factors.

Similar to Opdal et al. (2008) and Cox et al. (2013), this study could not detect an unequivocal effect of the ridge on backscattering strength. This may be because the ridge does not exert an effect on scattering layers at the vertical and geographical scale investigated. It contrasts with the observations of Priede et al. (2013), who present a notable increase of deep scattering layer biomass around the Reykjanes ridge at spatial scales of hundreds of km. However, Priede et al. (2013) ascribe this to behavioural associations with topography and not locally increased pelagic productivity, and argue that the effect of mid-ocean ridges on basin-scale total biomass is neutral. They do not present any data to support this, and no aggregating effect is apparent for the continental slopes in their dataset, casting some doubt on the aggregation versus enhanced productivity conjecture.

4.4 Diel variations in backscatter

Apart from temperature, time of day consistently exhibited pronounced effects on backscatter in all models. Generally model fits indicated high levels of backscatter during the day and lower levels during the night for the DSL, and the opposite pattern for the SSL. This pattern conforms to a DVM cycle with scatterers moving out of the mesopelagic zone and into the euphotic zone at night and returning to deeper water during day (Angel, 1985; O'Driscoll et al., 2009). However, the diel backscatter cycle was more complex, with the SSL exhibiting a secondary peak around local noon as well as a secondary trough at local midnight (Figs. 6D and 6B,C). The causes for this are less clear, although a possible explanation could again be scatterers migrating into and out of the surface dead zone during the extremes of the diel cycle. Some evidence supporting this is provided by the fact that the noon peak of the DVM cycle in the 18 kHz SSL was more pronounced in the "on SWIR" smooth, compared to the "off SWIR" smooth (Fig. 8B,C), which corresponds to a shallower and more intense SSL in the southern cluster D2, compared to the northern cluster D1 (Fig. 4D).

Vertical migrations within and between sampled volumes, however, may not be the only factors causing diel backscatter variations. The acoustic target strength, i.e. the propensity of a given target to reflect acoustic energy, can be strongly dependent on the aspect at which a target is insonified. Target strengths of mesopelagic fish can vary by several orders of magnitude between extreme tilt angles, i.e. horizontal vs. head up or head down (Benoit-Bird and Au, 2001; Yasuma et al., 2003, 2010), adding considerable uncertainty to acoustic biomass estimates (e.g. Demer, 2004). Observations of the *in situ* orientation of scattering layer organisms are scarce, but significant day-night differences in the orientation of myctophids and *Cyclothone* spp. have been reported from the Pacific (Barham, 1970). Furthermore, target strength is not independent of depth, as migrations through the hydrostatic depth gradient can alter swimbladder volume (Fässler et al., 2009). This can bias target strengths, in particular

near the resonance frequency, leading to artifical increases of backscatter at particular depths (Godø et al., 2009).

4.5 Conclusions and outlook

With programs like the IMOS Bio-Acoustic Subfacility, the amount of scattering layer data is likely to increase considerably in the future, and there is an imperative to try to make the most out of these data by using analysis frameworks that adequately address the inherent space-time variability. Fisheries acoustics are certainly not an unbiased sampling method for pelagic biota, but few, if any, sampling technologies can provide information across mid to high-trophic level biota with the same spatial and temporal coverage.

Overall the analyses reported here showed a heterogeneous distribution of pelagic backscatter across the southwest Indian Ocean. Variability in hydrographic features explained a large amount of the variation in the data, with increased backscatter at both the STF and SAF. No strong evidence of a ridge effect was found at the basin scale. Cluster analysis suggested the existence of structurally distinct scattering layer regimes north and south of the SAF, which together with differing S_v intensity patterns between the two frequencies south of the SAF, indicates that acoustic observations can indeed delineate biogeographical regions. Stratifying acoustic backscatter data into faunal provinces may increase the accuracy of acoustic biomass estimates on global scales, such as the recent estimate by Irigoien et al. (2014), which was based on globally averaged target strength-biomass relationships.

Tracking and biologging studies have highlighted the importance of the SWIO, and in particular the fronts south of the STF and into the Southern Ocean, as a foraging habitat for predators of mesopelagic fish. These predators include several million pairs of macaroni penguins *Eudyptes chrysolophus*, the single largest consumer among seabirds (Brooke, 2004; Thiebot et al., 2011), as well as southern

elephant seals *Mirounga leonina* (Bailleul et al., 2007; Dragon et al., 2010). It is likely that the elevated backscatter observed in the present study reflects the prey resources exploited by pelagic predators. Tracking data have furthermore indicated differences in elephant seal foraging behaviour and/or foraging success on either side of oceanic fronts (McIntyre et al., 2011; Boersch-Supan et al., 2012; Guinet et al., 2014), which likely demonstrates adaptive foraging behaviour in distinct pelagic biomes. This is to be expected given the distinct vertical SL (i.e prey-field) profiles that the present study has exposed.

GAMMs performed adequately, although they came with a high computational cost. Individual GAMMs for the full 38 kHz dataset took between 0.3 and 2.2 hrs to fit on a high-performance workstation (MacPro 5,1 with 12 processor cores and 48 GB of memory; Apple Inc., Cupertino, CA, USA), consuming about 7 GB of working memory in the process. GAMs for the same data but without a correlation structure were usually fitted in less than a minute. Computational limitations can probably be addressed by more efficient software and better hardware, but the quest for better analytical tools remains for acoustic data. This study addressed spatial and temporal correlation along the survey track, but was limited to a set of independent models with an arbitrary depth stratum of integrated backscatter as a response variable. This reduced ecological insight and left some uncertainty in the interpretation of model results, e.g. of the underlying causes for different time-of-day smooths. Ultimately the aim for analyses of SL data should be depth-explicit models that capture both geographical and vertical patterns in one unified framework. Such a model could be useful to produce spatially and temporally explicit predictions of SL density and diel vertical migration dynamics, which could in turn be used to parameterize ecosystem and biogeochemical flux models (e.g. Lehodey et al., 2008).

Acknowledgements

Ship of Opportunity Data were sourced from the Integrated Marine Observing System (IMOS) - an initiative of the Australian Government being conducted as part of the National Collaborative Research Infrastructure Strategy and the Super Science Initiative. Other acoustic data were collected as part of the Southwest Indian Ocean Seamounts Project (http://www.iucn.org/marine/seamounts) which was supported supported by the EAF Nansen Project, the Food and Agriculture Organization of the United Nations, the Global Environment Facility, the International Union for the Conservation of Nature, the Natural Environment Research Council (Grant NE/F005504/1), the Leverhulme Trust (Grant F00390C) and the Total Foundation.. We thank the Masters, officers, crews and science parties of cruises DFN 2009-410 and JCO66/67 for their assistance during echosounder calibration and data acquisition, and two anonymous reviewers for their comments. PHBS was supported by the German National Academic Foundation, a Cusanuswerk doctoral fellowship, and a Lesley & Charles Hilton-Brown Scholarship.

References

Akaike, H., 1973. Information theory and an extension of the maximum likelihood principle. *In* B. Petran and F. Csaaki (eds.) Second international symposium on information theory, pp. 267–281. Akademinai Kiado, Budapest, Hungary.

Al-Mutairi, H. and M. R. Landry, 2001. Active export of carbon and nitrogen at Station ALOHA by diel migrant zooplankton. *Deep Sea Research Part II: Topical Studies in Oceanography* **48**:2083–2103.

Anderson, C., A. Brierley, and F. Armstrong, 2005. Spatio-temporal variability in the distribution of epi- and meso-pelagic acoustic backscatter in the Irminger Sea, North Atlantic, with implications for predation on *Calanus finmarchicus*. *Marine Biology* **146**:1177–1188.

Angel, M., 1985. Vertical migrations in the oceanic realm: Possible causes and probable effects. *Contributions in Marine Science.* **27**:45–70.

Anon., 2010. ESA DUE GlobColour – Global Ocean Colour for Carbon Cycle Research, Product User Guide. ACRI-ST/LOV, UoP, NIVA, BC, DLR, ICESS consortium. Reference: GC-UM-ACR-PUG-01, Version 1.4.

Arranz, P., N. de Soto, P. Madsen, A. Brito, F. Bordes, and M. Johnson, 2011. Following a foraging fish-finder: Diel habitat use of Blainville's beaked whales revealed by echolocation. *PLoS ONE* **6**:e28353.

Backus, R. and J. Craddock, 1977. Pelagic faunal provinces and sound-scattering levels in the Atlantic Ocean. *In* N. Andersen and B. Zahuranec (eds.) Oceanic sound scattering prediction, *Marine Science*, vol. 5, pp. 529–547. Plenum Press, New York.

Bailleul, F., J. Charrassin, P. Monestiez, F. Roquet, M. Biuw, and C. Guinet, 2007. Successful foraging zones of southern elephant seals from the Kerguelen Islands in relation to oceanographic conditions. *Philosophical Transactions of the Royal Society B: Biological Sciences* **362**:2169–2181.

Barange, M., E. Pakhomov, R. Perissinotto, P. Froneman, H. Verheye, J. Taunton-Clark, and M. Lucas, 1998. Pelagic community structure of the subtropical convergence region south of Africa and in the mid-Atlantic Ocean. *Deep-Sea Research Part I* **45**:1663–1687.

Barham, E. G., 1970. Deep-sea fishes lethargy and vertical orientation. *In* G. Farquhar (ed.) Proceedings of an International Symposium on Biological Sound Scattering in the Ocean, pp. 100–118. Maury Center for Ocean Science, Washington, D.C.

Belkin, I. and A. Gordon, 1996. Southern Ocean fronts from the Greenwich meridian to Tasmania. *Journal of Geophysical Research* **101**:3675–3696.

Benoit-Bird, K. and W. Au, 2001. Target strength measurements of Hawaiian mesopelagic boundary community animals. *The Journal of the Acoustical Society of America* **110**:812–819.

Bianchi, D., C. Stock, E. D. Galbraith, and J. L. Sarmiento, 2013. Diel vertical migration: Ecological controls and impacts on the biological pump in a one-dimensional ocean model. *Global Biogeochemical Cycles* .

Boersch-Supan, P., L. Boehme, J. Read, A. Rogers, and A. Brierley, 2012. Elephant seal foraging dives track prey distributions, not temperature: Comment on McIntyre et al. (2011). *Marine Ecology Progress Series* **461**:293–298.

Bornman, T. G., M. J. Sonnekus, and E. E. Campbell, 2014. Phytoplankton and nutrient dynamics of six south indian seamounts. *Deep Sea Research II* .

Bradbury, M., D. Abbot, R. Bovbjerg, R. Mariscal, W. Fielding, R. Barber, V. Pearse, S. Proctor, J. Ogden, J. Wourms, L. Taylor Jr., J. Christofferson, J. Christofferson, R. McPhearson, M. Wynne, and P. Stromberg Jr., 1970. Studies on the fauna associated with the deep scattering layers in the equatorial Indian Ocean, conducted on R/V TE VEGA during October and November 1964. *In* G. Farquhar (ed.) Proceedings of an International Symposium on Biological Sound Scattering in the Ocean, pp. 409–452. Maury Center for Ocean Science, Washington, D.C.

Brooke, M. d. L., 2004. The food consumption of the world's seabirds. *Proceedings of the Royal Society of London. Series B: Biological Sciences* **271**:S246–S248.

Burgos, J. and J. Horne, 2008. Characterization and classification of acoustically detected fish spatial distributions. *ICES Journal of Marine Science* **65**:1235.

Butler, D., 2009. Ship decision sinks UK marine science, Nature News (23 March 2009) | doi:10.1038/458392a

Christensen, R., G. Duvall, and J. MW Johnson RL Ely, 1946. Stratification of sound scatterers in the sea. Tech. Rep. M397, University of California War Research Division, U.S. Navy Electronics Laboratory, San Diego, CA.

Ciannelli, L., P. Fauchald, K.-S. Chan, V. N. Agostini, and G. E. Dingsør, 2008. Spatial fisheries ecology: recent progress and future prospects. *Journal of Marine Systems* **71**:223–236.

Cisewski, B., V. Strass, M. Rhein, and S. Krägefsky, 2010. Seasonal variation of diel vertical migration of zooplankton from ADCP backscatter time series data in the Lazarev Sea, Antarctica. *Deep Sea Research Part I: Oceanographic Research Papers* **57**:78–94.

Coffin, M., L. Gahagan, and L. Lawver, 1998. Present-day plate boundary digital data compilation. Tech. Rep. 174, University of Texas Institute for Geophysics.

Cole, H., G. Bryan, and A. Gordon, 1970. The deep scattering layer: patterns across the Gulf Stream and the Sargasso Sea. *In* G. Farquhar (ed.) Proceedings of an International Symposium on Biological Sound Scattering in the Ocean, pp. 281–293. Maury Center for Ocean Science, Washington, D.C.

Conte, M., J. Bishop, and R. Backus, 1986. Nonmigratory, 12-kHz, deep scattering layers of Sargasso Sea origin in warm-core rings. *Deep-Sea Research Part A: Oceanographic Research Papers* **33**:1869–1884.

Corripio, J. G., 2013. insol: Solar Radiation. URL http://CRAN.R-project.org/package=insol. R package version 1.1.

Cox, M. J., T. B. Letessier, and A. S. Brierley, 2013. Zooplankton and micronekton biovolume at the Mid-Atlantic Ridge and Charlie-Gibbs Fracture Zone estimated by multi-frequency acoustic survey. *Deep Sea Research II* In press; http://dx.doi.org/10.1016/j.dsr2.2013.07.020.

De Robertis, A. and I. Higginbottom, 2007. A post-processing technique to estimate the signal-to-noise ratio and remove echosounder background noise. *ICES Journal of Marine Science* **64**:1282.

Demer, D., 2004. An estimate of error for the CCAMLR 2000 survey estimate of krill biomass. *Deep Sea Research II* **51**:1237–1251.

Djurhuus, A., J. F. Read, and A. D. Rogers, 2014. The spatial distribution of particulate organic carbon and microorganisms on seamounts of the south west indian ridge. *Deep Sea Research II* .

Donlon, C. J., M. Martin, J. Stark, J. Roberts-Jones, E. Fiedler, and W. Wimmer, 2012. The operational sea surface temperature and sea ice analysis (OSTIA) system. *Remote Sensing of Environment* **116**:140–158.

Dragon, A., P. Monestiez, A. Bar-Hen, and C. Guinet, 2010. Linking foraging behaviour to physical oceanographic structures: Southern elephant seals and mesoscale eddies east of Kerguelen Islands. *Progress in Oceanography* **87**:61–71.

Falkowski, P. and Z. Kolber, 1995. Variations in chlorophyll fluorescence yields in phytoplankton in the world oceans. *Australian Journal of Plant Physiology* **22**:341–355.

Farquhar, G., 1977. Biological sound scattering in the oceans: a review. *In* N. Andersen and B. Zahuranec (eds.) Oceanic sound scattering prediction, *Marine Science*, vol. 5, pp. 493–527. Plenum Press, New York.

Fässler, S.M., Fernandes, P.G., Semple, S.I., and Brierley, A.S., 2009. Depth-dependent swimbladder compression in herring Clupea harengus observed using magnetic resonance imaging. *Journal of Fish Biology* **74**:296-303.

Fernandes, P. G., F. Gerlotto, D. V. Holliday, O. Nakken, and E. J. Simmonds, 2002. Acoustic applications in fisheries science: the ICES contribution. *ICES Marine Science Symposia* **215**:483–492.

Fofonoff, N. and R. Millard, 1983. Algorithms for computation of fundamental properties of seawater. *Unesco Technical Papers in Marine Science* **44**:46–50.

Foote, K., H. Knudsen, G. Vestnes, D. MacLennan, and E. Simmonds, 1987. Calibration of acoustic instruments for fish density estimation: a practical guide. *ICES Cooperative Research Reports* **144**:69.

GEBCO, 2010. General Bathymetric Chart of the Oceans – The GEBCO 08 Grid. Version 20100927, http://www.gebco.net.

Genin, A., 2004. Bio-physical coupling in the formation of zooplankton and fish aggregations over abrupt topographies. *Journal of Marine Systems* **50**:3–20.

Genin, A., P. Dayton, P. Lonsdale, and F. Spiess, 1986. Corals on seamount peaks provide evidence of current acceleration over deep-sea topography. *Nature* **322**:59–61.

Godø, O., R. Patel, and G. Pedersen, 2009. Diel migration and swimbladder resonance of small fish: some implications for analyses of multifrequency echo data. *ICES Journal of Marine Science* **66**:1143.

Godø, O. R., A. Samuelsen, G. J. Macaulay, R. Patel, S. S. Hjøllo, J. Horne, S. Kaartvedt, and J. A. Johannessen, 2012. Mesoscale eddies are oases for higher trophic marine life. *PLoS ONE* **7**:e30161.

Gower, J. C., 1971. A general coefficient of similarity and some of its properties. *Biometrics* **27**:857–871.

Guinet, C., J. Vacquié-Garcia, B. Picard, G. Bessigneul, Y. Lebras, A. C. Dragon, M. Viviant, J. P. Arnould, and F. Bailleul, 2014. Southern elephant seal foraging success in relation to temperature and light conditions: insight into prey distribution. *Marine Ecology Progress Series* **499**:285–301.

Haury, L., J. McGowan, and P. Wiebe, 1978. Patterns and processes in the time-space scales of plankton distributions. *In* J. Steele (ed.) Spatial pattern in plankton communities, *NATO Conference Series in Marine Sciences*, vol. 3, pp. 277–327. Plenum Press, New York, NY.

Hazen, E. and D. Johnston, 2010. Meridional patterns in the deep scattering layers and top predator distribution in the central equatorial Pacific. *Fisheries Oceanography* **19**:427–433.

Hidaka, K., K. Kawaguchi, M. Murakami, and M. Takahashi, 2001. Downward transport of organic carbon by diel migratory micronekton in the western equatorial Pacific: its quantitative and qualitative importance. *Deep Sea Research I* **48**:1923–1939.

Hijmans, R. J. and J. van Etten, 2012. raster: Geographic data analysis and modeling. URL http://CRAN.R-project.org/package=raster. R package version 2.0-41.

Hijmans, R. J., E. Williams, and C. Vennes, 2012. geosphere: Spherical Trigonometry. URL http://CRAN.R-project.org/package=geosphere. R package version 1.2-28.

Howey-Jordan, L. A., E. J. Brooks, D. L. Abercrombie, L. K. Jordan, A. Brooks, S. Williams, E. Gospodarczyk, and D. D. Chapman, 2013. Complex movements, philopatry and expanded depth range of a severely threatened pelagic shark, the oceanic whitetip (*Carcharhinus longimanus*) in the western North Atlantic. *PLoS ONE* **8**:e56588.

Irigoien, X., T. Klevjer, A. Røstad, U. Martinez, G. Boyra, J. Acuña, A. Bode, F. Echevarria, J. Gonzalez-Gordillo, S. Hernandez-Leon, S. Agusti, D. Aksnes, C. Duarte, and S. Kaartvedt, 2014. Large mesopelagic fishes biomass and trophic efficiency in the open ocean. *Nature communications* **5**.

Isaacs, J. and R. Schwartzlose, 1965. Migrant sound scatterers: interaction with the sea floor. *Science* **150**:1810–1813.

Kaartvedt, S., A. Staby, and D. Aksnes, 2012. Efficient trawl avoidance by mesopelagic fishes causes large underestimation of their biomass. *Marine Ecology Progress Series* **456**:1–6.

Kaufman, L. and P. J. Rousseeuw, 1990. Finding groups in data: an introduction to cluster analysis. Wiley, New York.

Kemp, K. M., P. H. Boersch-Supan, O. Alvheim, D. Benivary, V. Mangar, and A. D. Rogers, 2014. Pelagic fish community composition of the south west indian ocean ridge. *Deep Sea Research II* .

Kim, S.-S. and P. Wessel, 2011. New global seamount census from altimetry-derived gravity data. *Geophysical Journal International* **186**:615–631.

Klevjer, T. A., D. J. Torres, and S. Kaartvedt, 2012. Distribution and diel vertical movements of mesopelagic scattering layers in the red sea. *Marine Biology* **159**:1833–1841.

Kloser, R., T. Ryan, J. Young, and M. Lewis, 2009. Acoustic observations of micronekton fish on the scale of an ocean basin: potential and challenges. *ICES Journal of Marine Science* **66**:998.

Koslow, J., 1997. Seamounts and the ecology of deep-sea fisheries. *American Scientist* **85**:168–176.

Laptikovsky, V., P. Boersch-Supan, K. Kemp, T. Letessier, and A. Rogers, 2014. Cephalopods of the Southwest Indian Ocean Ridge: a hotspot of extreme biological diversity and absence of endemism. Unpublished manuscript.

Lara-Lopez, A., P. Davison, and J. Koslow, 2012. Abundance and community composition of micronekton across a front off Southern California. *Journal of Plankton Research* **34**:828–848.

Legendre, P., 1993. Spatial autocorrelation: trouble or new paradigm? *Ecology* **74**:1659–1673.

Lehodey, P., R. Murtugudde, and I. Senina, 2010. Bridging the gap from ocean models to population dynamics of large marine predators: a model of mid-trophic functional groups. *Progress in Oceanography* **84**:69–84.

Lehodey, P., I. Senina, and R. Murtugudde, 2008. A spatial ecosystem and populations dynamics model (seapodym)–modeling of tuna and tuna-like populations. *Progress in Oceanography* **78**:304–318.

Letessier, T., S. De Grave, P. Boersch-Supan, K. Kemp, A. Brierley, and A. Rogers, 2014. The biogeography of pelagic shrimps (Decapoda) and Gnathophausiids (Lophogastridea) on seamounts of the South-West Indian Ocean Ridge. Unpublished manuscript.

Lewin-Koh, N. J. and R. Bivand, 2010. maptools: Tools for reading and handling spatial objects. URL http://CRAN.R-project.org/package=maptools. R package version 0.7-34.

Longhurst, A., 1998. Ecological Geography of the Sea. Academic Press, San Diego CA, USA.

Longhurst, A., S. Sathyendranath, T. Platt, and C. Caverhill, 1995. An estimate of global primary production in the ocean from satellite radiometer data. *Journal of Plankton Research* **17**:1245–1271.

Lyman, J., 1947. The sea's phantom bottom. *The Scientific Monthly* **66**:87–88.

MacLennan, D. N., P. G. Fernandes, and J. Dalen, 2002. A consistent approach to definitions and symbols in fisheries acoustics. *ICES Journal of Marine Science* **59**:365–369.

Maechler, M., P. Rousseeuw, A. Struyf, M. Hubert, and K. Hornik, 2012. cluster: Cluster Analysis Basics and Extensions. R package version 1.14.3.

McClatchie, S., G. Macaulay, and R. Coombs, 2004. Acoustic backscatter and copepod secondary production across the Subtropical Front to the east of New Zealand. *Journal of Geophysical Research* **109**:C03013.

McIntyre, T., I. Ansorge, H. Bornemann, J. Plötz, C. Tosh, and M. Bester, 2011. Elephant seal dive behaviour is influenced by ocean temperature: implications for climate change impacts on an ocean predator. *Marine Ecology Progress Series* **441**:257–272.

Meeus, J., 1998. Astronomical algorithms. Willmann-Bell, Richmond, Va.

Morato, T., C. Bulman, and T. Pitcher, 2009. Modelled effects of primary and secondary production enhancement by seamounts on local fish stocks. *Deep Sea Research II* **56**:2713–2719.

Morato, T., D. Varkey, C. Damaso, M. Machete, M. Santos, R. Prieto, R. Santos, and T. Pitcher, 2008. Evidence of a seamount effect on aggregating visitors. *Marine Ecology Progress Series* **357**:23–32.

Murase, H., T. Kitakado, T. Hakamada, K. Matsuoka, S. Nishiwaki, and M. Naganobu, 2013. Spatial distribution of Antarctic minke whales (*Balaenoptera bonaerensis*) in relation to spatial distributions of krill in the Ross Sea, Antarctica. *Fisheries Oceanography* **22**:154–173.

Nagpaul, P., 1999. Guide to advanced data analysis using IDAMS software. UNESCO, Paris.

Naito, Y., D. P. Costa, T. Adachi, P. W. Robinson, M. Fowler, and A. Takahashi, 2013. Unravelling the mysteries of a mesopelagic diet: a large apex predator specializes on small prey. *Functional Ecology* **27**:710–717.

Neteler, M., M. Bowman, M. Landa, and M. Metz, 2011. GRASS GIS: a multi-purpose open source GIS. *Environmental Modelling & Software* **31**:124–130.

O'Driscoll, R., S. Gauthier, and J. Devine, 2009. Acoustic estimates of mesopelagic fish: as clear as day and night? *ICES Journal of Marine Science* **66**:1310–1317.

Ohman, M., D. Rudnick, A. Chekalyuk, R. Davis, R. Feely, M. Kahru, H.-J. Kim, M. Landry, T. Martz, C. Sabine, and U. Send, 2013. Autonomous ocean measurements in the california current ecosystem. *Oceanography* **26**:18–25.

Opdal, A., O. Godø, O. Bergstad, and Ø. Fiksen, 2008. Distribution, identity, and possible processes sustaining meso-and bathypelagic scattering layers on the northern Mid-Atlantic Ridge. *Deep-Sea Research Part II* **55**:45–58.

Pakhomov, E., R. Perissinotto, and C. McQuaid, 1994. Comparative structure of the macrozooplankton / micronekton communities of the Subtropical and Antarctic Polar Fronts. *Marine Ecology Progress Series* **111**:155–169.

Pakhomov, E. A. and P. W. Froneman, 2000. Composition and spatial variability of macroplankton and micronekton within the antarctic polar frontal zone of the indian ocean during austral autumn 1997. *Polar Biology* **23**:410–419.

Pearre, S., 2003. Eat and run? The hunger/satiation hypothesis in vertical migration: history, evidence and consequences. *Biological Reviews* **78**:1–79.

Petitgas, P., 2001. Geostatistics in fisheries survey design and stock assessment: models, variances and applications. *Fish and Fisheries* **2**:231–249.

Pinheiro, J. and D. Bates, 2000. Mixed-effects models in S and S-PLUS. Springer, New York, NY u.a.

Pitcher, T., M. Clark, T. Morato, and R. Watson, 2010. Seamount fisheries: Do they have a future. *Oceanography* **23**:134–144.

Potier, M., F. Marsac, Y. Cherel, V. Lucas, R. Sabatié, O. Maury, and F. Ménard, 2007. Forage fauna in the diet of three large pelagic fishes (lancetfish, swordfish and yellowfin tuna) in the western equatorial Indian Ocean. *Fisheries Research* **83**:60–72.

Potier, M., F. Marsac, V. Lucas, R. Sabatié, J. Hallier, and F. Ménard, 2005. Feeding partitioning among tuna taken in surface and mid-water layers: The case of yellowfin (*Thunnus albacares*) and bigeye (*T. obesus*) in the western tropical Indian Ocean. *Western Indian Ocean Journal of Marine Science* **3**:51–62.

Priede, I. G., O. A. Bergstad, P. I. Miller, M. Vecchione, A. Gebruk, T. Falkenhaug, D. S. Billett, J. Craig, A. C. Dale, M. A. Shields, et al., 2013. Does presence of a mid-ocean ridge enhance biomass and biodiversity? *PLoS ONE* **8**:e61550.

R Development Core Team, 2010. R: A Language and Environment for Statistical Computing. R Foundation for Statistical Computing, Vienna, Austria. URL http://www.R-project.org.

Rivoirard, J., J. Simmonds, K. Foote, P. Fernandes, and N. Bez, 2000. Geostatistics for estimating fish abundance. Wiley-Blackwell, Oxford, UK.

Rousseeuw, P. J., 1987. Silhouettes: a graphical aid to the interpretation and validation of cluster analysis. *Journal of Computational and Applied Mathematics* **20**:53–65.

Rowden, A. A., T. A. Schlacher, A. Williams, M. R. Clark, R. Stewart, F. Althaus, D. A. Bowden, M. Consalvey, W. Robinson, and J. Dowdney, 2010. A test of the seamount oasis hypothesis: seamounts support higher epibenthic megafaunal biomass than adjacent slopes. *Marine Ecology* **31**:95–106.

Ryan, T., 2011. Overview of data collection, management and processing procedures of underway acoustic data - IMOS BASOOP sub-facility. CSIRO, Division of Marine and Atmospheric Research - Hobart, Australia. Version 1.0.

Ryan, T. and R. Kloser, 2004. Improving the precision of ES60 and EK60 echosounder applications. Tech. Rep. CM 2004/B:06, ICES Working Group on Fisheries Acoustic Science and Technology.

Steele, J., 1978. Some Comments on Plankton Patches. *In* J. Steele (ed.) Spatial pattern in plankton communities, *NATO Conference Series in Marine Sciences*, vol. 3, pp. 1–20. Plenum Press, New York, NY.

Steinberg, D. K., B. A. V. Mooy, K. O. Buesseler, P. W. Boyd, T. Kobari, and D. M. Karl, 2008. Bacterial vs. zooplankton control of sinking particle flux in the ocean's twilight zone. *Limnology and Oceanography* **53**:1327.

Thiebot, J.-B., Y. Cherel, P. N. Trathan, and C.-A. Bost, 2011. Inter-population segregation in the wintering areas of macaroni penguins. *Marine Ecology Progress Series* **421**:279–290.

Tont, S., 1976. Deep scattering layers: patterns in the Pacific. *CalCOFI Reports* **18**:112–117.

Tseytlin, V., 1985. The energetics of fish populations inhabiting seamounts. *Oceanology* **25**:237–239.

Urmy, S., J. Horne, and D. Barbee, 2012. Measuring the vertical distributional variability of pelagic fauna in Monterey Bay. *ICES Journal of Marine Science* **69**:184–196.

Vierros, M., I. Cresswell, E. E. Briones, J. Rice, and J. Ardron (eds.) 2009. Global Open Oceans and Deep Seabed (GOODS) - Biogeographic Classification, *IOC Technical Series*, vol. 84. UNESCO-IOC, Paris, France.

Wood, S., 2006. Generalized Additive Models: An Introduction with R. Chapman & Hall, London, UK.

Yasuma, H., K. Sawada, T. Ohshima, K. Miyashita, and I. Aoki, 2003. Target strength of mesopelagic lanternfishes (family Myctophidae) based on swimbladder morphology. *ICES Journal of Marine Science* **60**:584–591.

Yasuma, H., K. Sawada, Y. Takao, K. Miyashita, and I. Aoki, 2010. Swimbladder condition and target strength of myctophid fish in the temperate zone of the Northwest Pacific. *ICES Journal of Marine Science* **67**:135–144.

Yesson, C., M. R. Clark, M. L. Taylor, and A. D. Rogers, 2011. The global distribution of seamounts based on 30-second bathymetry data. *Deep Sea Research I* **58**:442–453.

Zender, C. S., 2008. Analysis of self-describing gridded geoscience data with netCDF Operators (NCO). *Environmental Modelling & Software* **23**:1338–1342.

Zwolinski, J., P. G. Fernandes, V. Marques, and Y. Stratoudakis, 2009. Estimating fish abundance from acoustic surveys: calculating variance due to acoustic backscatter and length distribution error. *Canadian Journal of Fisheries and Aquatic Sciences* **66**:2081–2095.

Table 1: Breakdown of along-track sampling units of 1km length retained for analysis by data source, frequency, time of day and season. Numbers in brackets give the numbers of individual calendar days for which data were collected.

		38kHz				18kHz		
		IMOS	JCO	DFN	Σ	JCO	DFN	Σ
Time of day	Day	10335	93	2641	13069	150	2641	2791
	Night	9980	70	1811	11861	91	1811	1902
	Twilight	6922	45	1509	8476	93	1509	1602
	Σ	27237	208	5961	**33406**	334	5961	**6295**
Season	Austral Summer	14795	208	5961	20964	334	5961	6295
		(38)	(16)	(26)	(80)	(16)	(26)	(42)
	Austral Winter	12442	0	0	12442	0	0	0
		(31)	(0)	(0)	(31)	(0)	(0)	(0)
	Σ	27237	208	5961	**33406**	334	5961	**6295**
		(69)	(16)	(26)	**(111)**	(16)	(26)	**(42)**

Table 2: Explanatory variables and corresponding parameters for the GAMMs used to model mean volume backscatter S_V in the deep and shallow scattering layers.

	Dependent variable			
	38 kHz		18 kHz	
	S_v^{DSL38}	S_v^{SSL38}	S_v^{DSL18}	S_v^{SSL18}
Parametric terms[a]				
(Intercept)	-76.918***	-73.031***	-75.587***	-73.407***
	(0.154)	(0.306)	(0.0565)	(0.2691)
Depth		2.64×10^{-4}**		
		(7.33×10^{-5})		
Smooth terms[b]				
s(SST):Summer	7.999***	8.195***	8.565***	6.422**
	(85.59)	(52.38)	(48.70)	(3.665)
s(SST):Winter[d]	6.940***	8.329***		
	(24.28)	(95.48)		
s(Time of day)	5.905***	7.873***		
	(17.75)	(240.41)		
s(Time of day):OnSWIR			7.168***	7.610***
			(19.66)	(75.20)
s(Time of day):OffSWIR			6.699***	7.320***
			(24.77)	(28.70)
s(Depth)			6.743***	2.825***
			(17.07)	(9.717)
s(DistRidge)		1.929***	8.023***	
		(24.61)	(22.00)	
s(DistCoast)	8.735***		7.589***	
	(22.20)		(12.87)	
Terms excluded from all models during model selection				
Chlorophyll				
AR(1) correlation coefficient[c]				
φ	0.985	0.936	0.815	0.943
	(0.983,0.987)	(0.931,0.940)	(0.792,0.836)	(0.933,0.952)
Other measures				
AIC	38 418	100 150	15 380	20 389
r^2_{adj}	0.356	0.663	0.732	0.545
Num. obs.	32 456	32 456	6 166	6 166

*** p < 0.0001, ** p < 0.001, * p < 0.01

[a] parameter estimate (std. error)

[b] effective degrees of freedom (F)

[c] parameter estimate (95% CI)

[d] 18 kHz data were only collected during Austral Summer

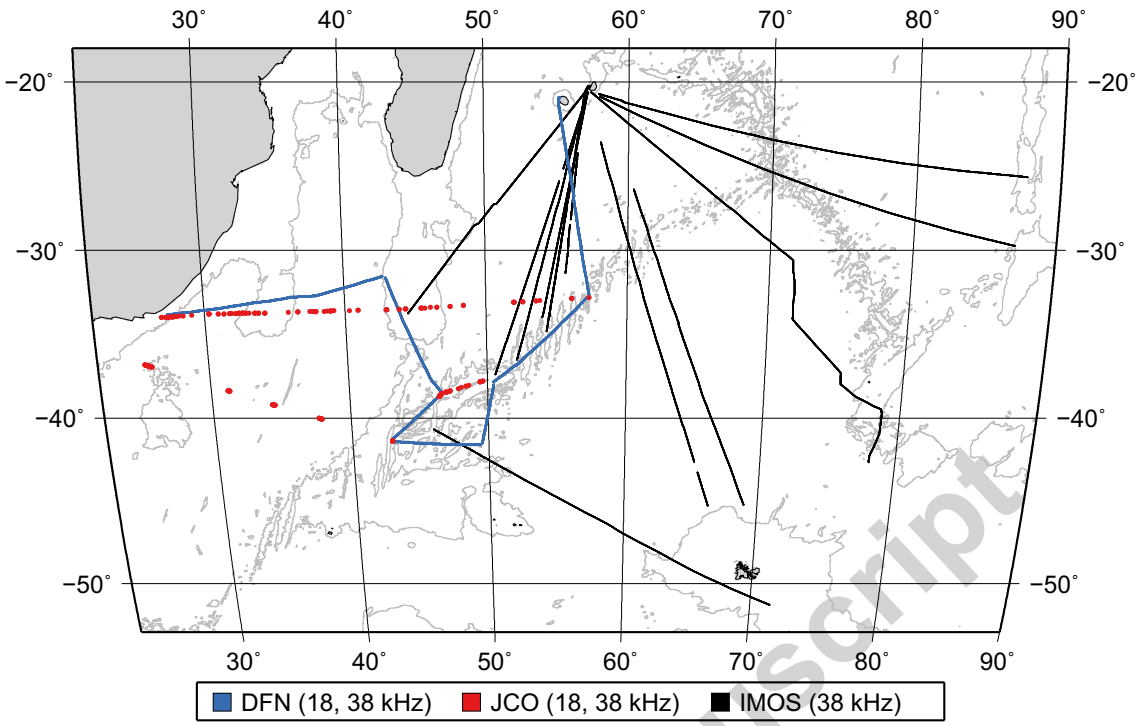

Figure 1: Sampling locations, frequencies and sources of acoustic data used in this study. Colours encode the project responsible for sampling. 3000m isobath traced from GEBCO (2010). DFN: *RV Dr. Fridtjof Nansen* Cruise 2009-410; JCO: *RRS James Cook* Cruise 66/67; IMOS: Australian Integrated Marine Observing System, Ships of Opportunity Bio-Acoustic sub-facility.

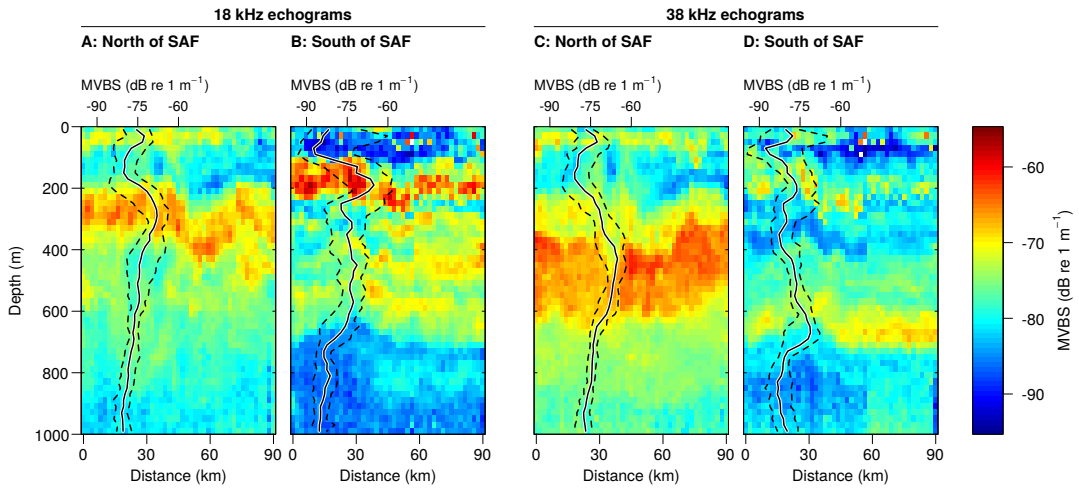

Figure 2: The vertical structure of daytime pelagic scattering layers in different parts of the survey area. Representative echograms are overlaid by vertical profiles illustrating the 2.5th, 50th and 97.5th percentile of the backscatter data shown in each panel. (A, C) Mean volume-backscattering strength north of the Subantarctic Front (SAF); (C,D) Mean volume-backscattering strength south of the SAF.

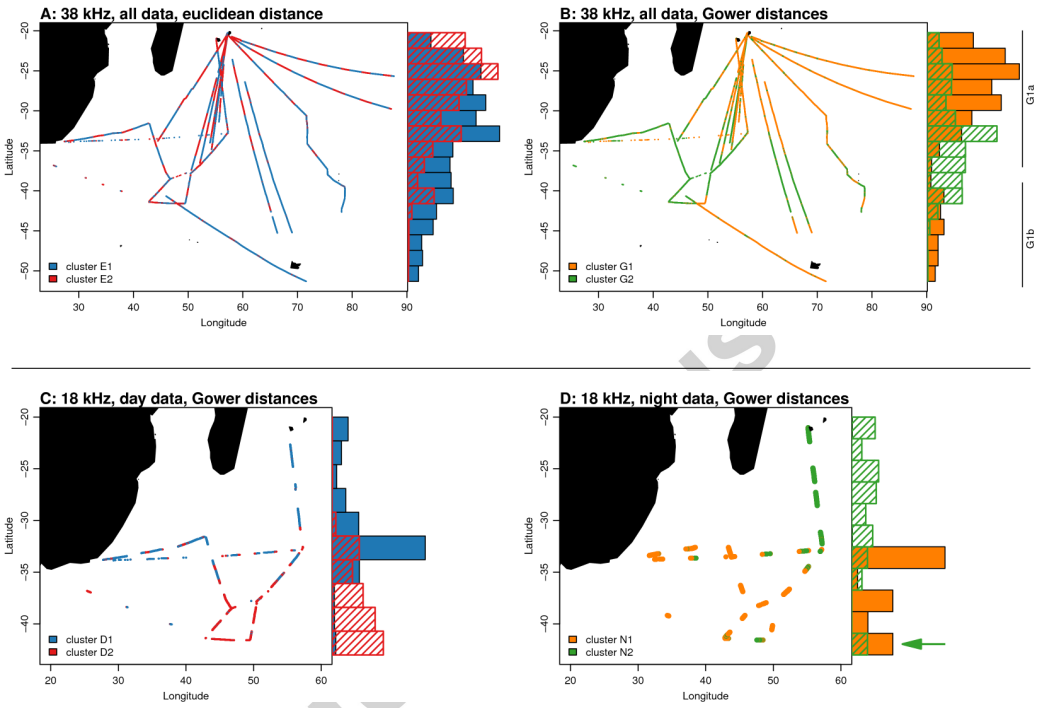

Figure 3: Maps of cluster allocations for the 38 kHz and 18 kHz datasets. Marginal histograms visualize the latitudinal composition of each cluster. In all cases $k = 2$ was the optimal partition. A: Euclidean distances partition the 38 kHz S_v profiles into a daytime and a nighttime cluster (cf. Fig. S3). B: Gower's distance metric partitions the data into two clusters, of which G1 is geographically discontinuous and can be separated into two sub-clusters G1a and G1b. C: The partitioning of daytime 18 kHz S_v profiles based on Gower's metric splits the dataset into a northern and southern cluster. D: The partition of nighttime S_v profiles largely corresponds to that of the daytime data. The green arrow highlights a transect section near 42°S 48°E classified as belonging to the northern cluster N2.

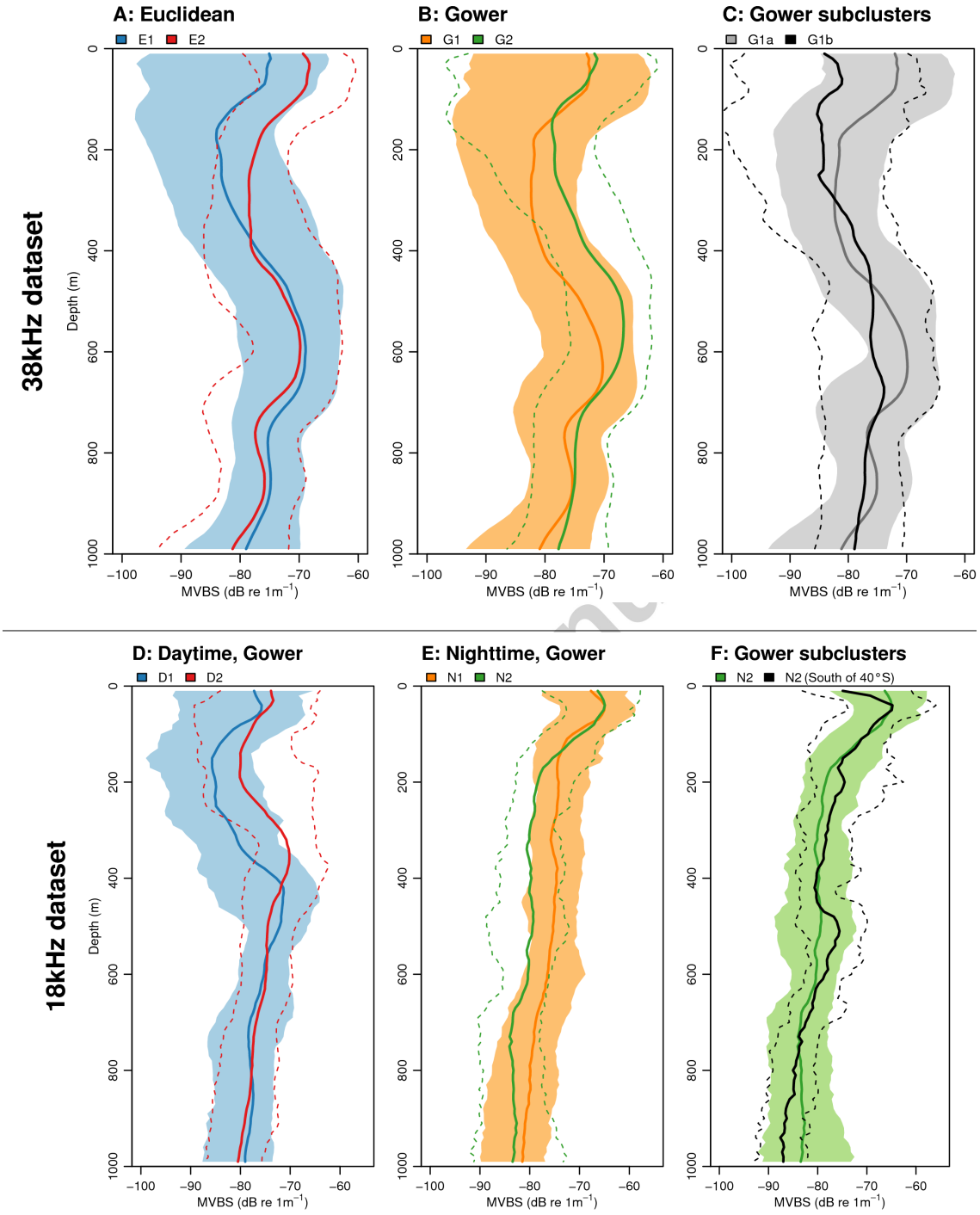

Figure 4: Vertical S_v profiles (2.5^{th}, 50^{th} and 97.5^{th} percentile) for the clusters mapped in Figure 3. A: Day/night split achieved by euclidean distances. B: Geographic split achieved by the Gower distance metric. C: Geographic subclusters derived from G1. D: Geographic split achieved within the 18 kHz daytime data. E: Geographic split achieved within the 18 kHz nighttime data. D: Subcluster derived from N2.

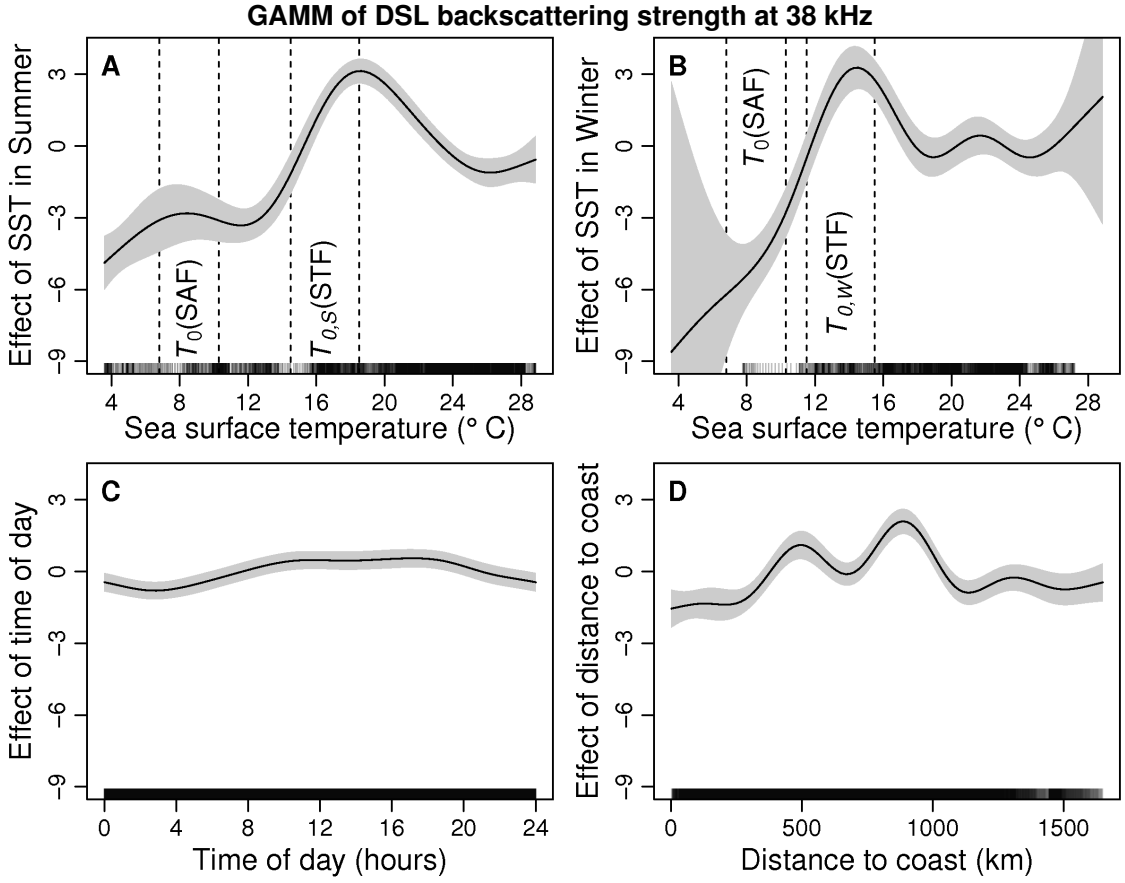

Figure 5: Smooths of generalized additive model terms showing the effect of various continuous variables on DSL backscattering strength at 38 kHz. The solid lines are the estimates of the smooths, the shaded areas are standard errors of the estimated smooths, taking into account the error in the model intercept. Dashed vertical lines in panel A and B indicate the axial temperature ranges T_0 of the subantarctic (SAF) and subtropical fronts (STF), respectively (Belkin and Gordon, 1996). Subscripts S and W, denote STF Summer and Winter T_0 ranges, respectively.

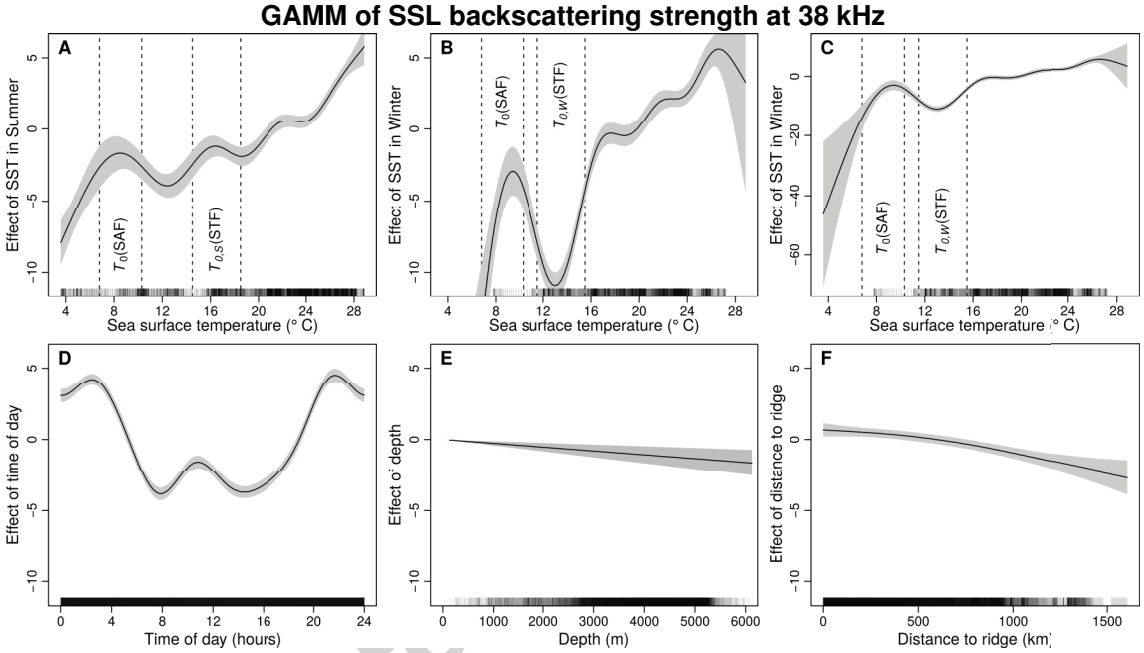

Figure 6: Smooths of generalized additive model terms showing the effect of various continuous variables on SSL backscattering strength at 38 kHz. The solid lines are the estimates of the smooths, the shaded areas are standard errors of the estimated smooths, taking into account the error in the model intercept. Panels B and C show the same smooth term, but with different y-axis scales. Dashed vertical lines in panel A and B indicate the axial temperature ranges T_0 of the subantarctic (SAF) and subtropical fronts (STF), respectively (Belkin and Gordon, 1996). Subscripts S and W, denote STF Summer and Winter T_0 ranges, respectively.

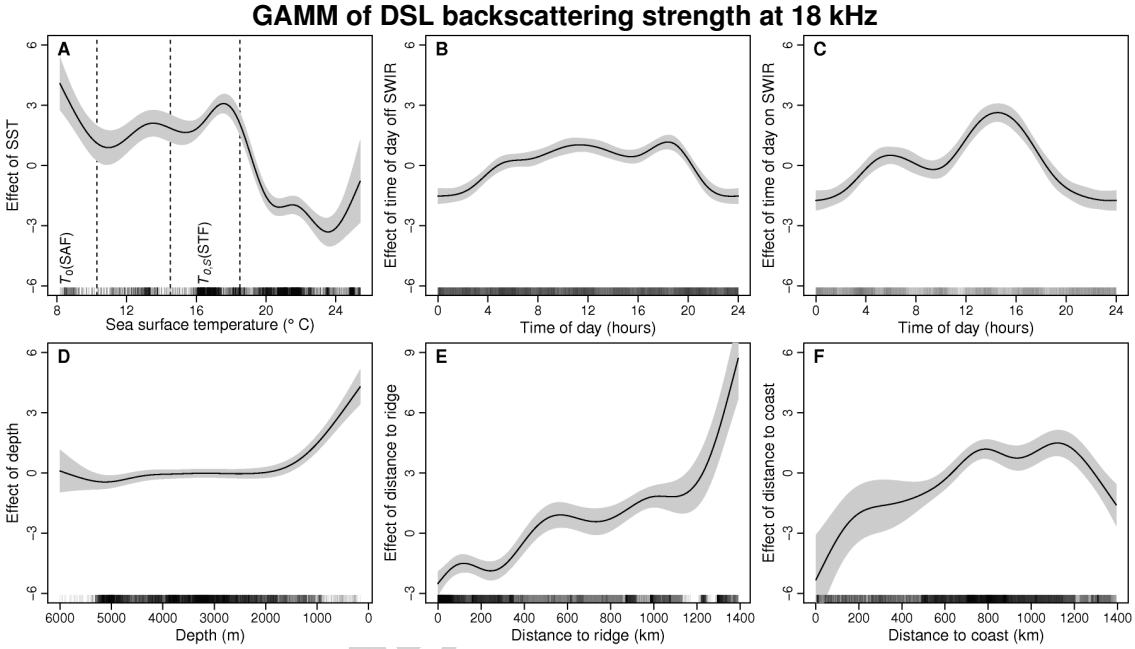

Figure 7: Smooths of generalized additive model terms showing the effect of various continuous variables on DSL backscattering strength at 18 kHz. The solid lines are the estimates of the smooths, the shaded areas are standard errors of the estimated smooths, taking into account the error in the model intercept. The y-axis of panel D is shifted relative to the remaining panels to accommodate the range of the effect, but the scale is not altered. Dashed vertical lines in panel A and B indicate the axial temperature ranges T_0 of the subantarctic (SAF) and subtropical fronts (STF), respectively (Belkin and Gordon, 1996).

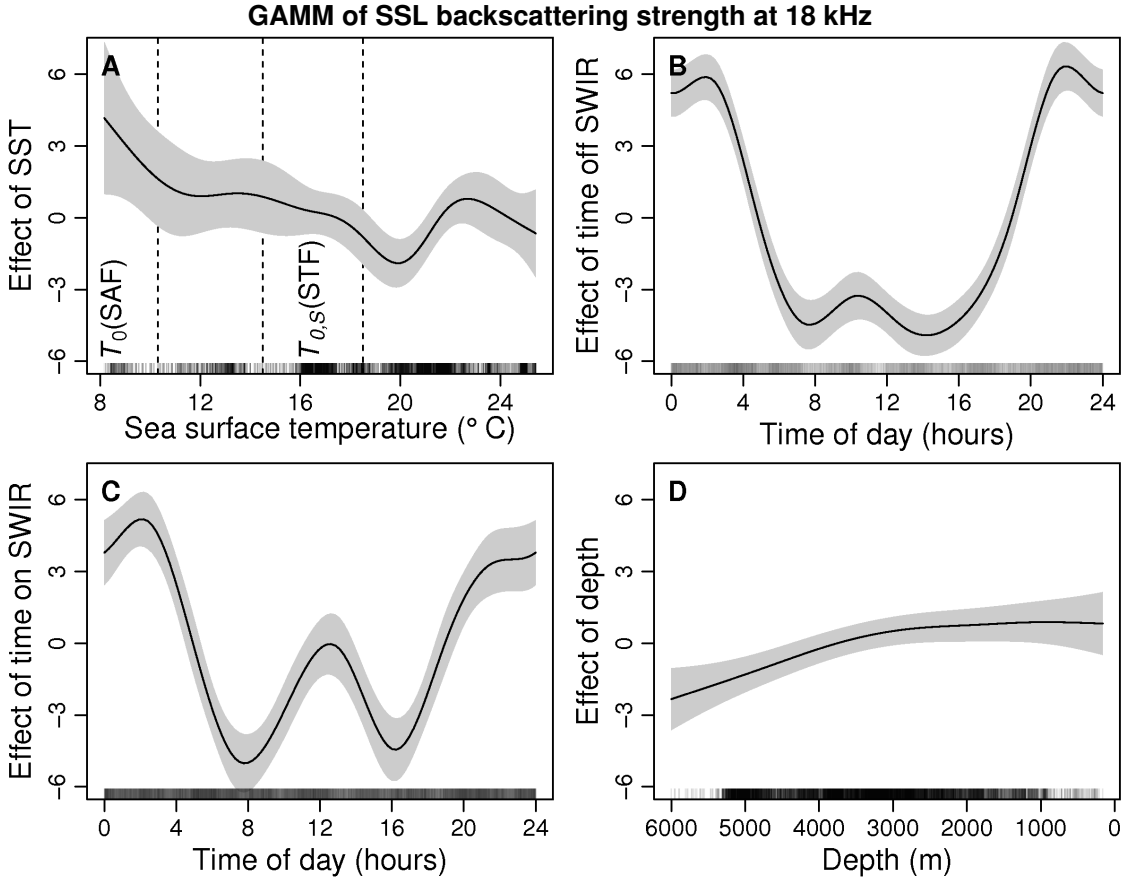

Figure 8: Smooths of generalized additive model terms showing the effect of various continuous variables on SSL backscattering strength at 18 kHz. The solid lines are the estimates of the smooths, the shaded areas are standard errors of the estimated smooths, taking into account the error in the model intercept. Dashed vertical lines in panel A and B indicate the axial temperature ranges T_0 of the subantarctic (SAF) and subtropical fronts (STF), respectively (Belkin and Gordon, 1996).